Available online at www.sciencedirect.com
SCIENCE DIRECT®
Journal of Computational Physics 215 (2006) 430–447
JOURNAL OF COMPUTATIONAL PHYSICS
www.elsevier.com/locate/jcp

A mass-conserving vorticity–velocity formulation with application to nonreacting and reacting flows

S.B. Dworkin *, B.A.V. Bennett, M.D. Smooke

Yale University, Department of Mechanical Engineering, P.O. Box 208284, 15 Prospect Street, New Haven, CT 06520-8284, USA

Received 13 April 2005; received in revised form 5 October 2005; accepted 1 November 2005
Available online 13 December 2005

Abstract

In a commonly implemented version of the vorticity–velocity formulation, the governing equations for the fluid dynamics are expressed as two Poisson-like velocity equations together with the vorticity transport equation. However, for some flows with large vorticity gradients, spurious mass loss or gain can be observed. In order to conserve mass, a modification to the vorticity–velocity formulation is proposed, involving the substitution of the kinematic definition of vorticity in certain terms of the fluid-dynamic equations. This modified formulation results in a broader computational stencil when the equations are in a second-order-accurate discretized form, and a stronger coupling between the predicted vorticity and the curl of the predicted velocity field. The resulting system of elliptic equations – which includes the energy and species transport equations for the reacting flow case – is discretized with finite differences on a nonstaggered grid and is then solved using Newton's method. Both the unmodified and modified vorticity–velocity formulations are applied to two problems with high vorticity gradients: (1) incompressible, axisymmetric fluid flow through a suddenly expanding pipe and (2) a confined, axisymmetric laminar flame with detailed chemistry and multicomponent transport, generated on a burner whose inner tube extends above the burner surface. The modified formulation effectively eliminates the spurious mass loss in the two test cases to within an acceptable tolerance. The two cases demonstrate the broader range of applicability of the modified formulation, as compared with the unmodified formulation.

MSC: 65N22; 76M20

PACS: ; 47.11.+j

Keywords: Vorticity–velocity; Implicit solver; Newton's method; Suddenly expanding pipe; Chemically reacting flow

1. Introduction

The aim of the present work is to extend the applicability of the vorticity–velocity formulation of the fluid-dynamic equations to numerical simulations that have previously demonstrated an appreciable spurious mass

* Corresponding author. Tel.: +1 203 432 0198; fax: +1 203 432 6775.
E-mail address: seth.dworkin@yale.edu (S.B. Dworkin).

0021-9991/$ - see front matter
doi:10.1016/j.jcp.2005.11.002

loss or gain. This paper focuses on the solution of the vorticity transport equation with two Poisson-like velocity equations in cylindrical coordinates for axisymmetric problems on nonstaggered grids. When one or more solid protrusions are introduced, such as a corner of a suddenly expanding pipe in a nonreacting flow, or the solid end of an extended reactant tube in a chemically reacting flow, these protrusions can generate large gradients in vorticity (an order of magnitude larger than those observed in simulations without solid protrusions), which can often prevent continuity from being satisfied, even within a converged solution. With an eye toward simulating flames in geometrically practical configurations, the modified vorticity–velocity formulation developed here ensures continuity and it is an important step toward enabling the simulation of reacting flow with detailed chemistry for a broader range of burner geometries. To obtain rapidly converging, accurate solutions, a fully implicit solver is used for the calculations presented in this paper, since it has proven to be more computationally efficient than explicit solution methods [1].

Based on a review of the vorticity–velocity formulation and its application in fluid flow computations [2], one can identify three common versions of the formulation that are currently in use. All three employ the vorticity transport equation, which is derived by taking the curl of the momentum conservation equations. In addition, all three are attractive because pressure is eliminated from the fluid-dynamic equations, and thus pressure boundary conditions do not need to be specified. However, the versions differ in their choice of equations used to describe the velocity field. The first is the integro-differential approach, which involves an integral formulation of the continuity and vorticity equations and was developed in the early 1970s by Wu and Thomson [3]. This version of the formulation has generated flow solutions that agree well with experimental and other computational results for many time-dependent, two-dimensional aerodynamic flow problems. The second version, in the form of a Cauchy–Riemann system, describes the velocity field using the continuity equation and the kinematic definition of vorticity (i.e., vorticity equals the curl of velocity). In [4], Gatski et al. have applied this approach successfully with compact finite-difference schemes, solving both two-dimensional (2D) and three-dimensional (3D) stagnation point and driven cavity flows. While both of these versions of the formulation satisfy continuity explicitly, neither version is particularly well suited to a fully implicit solver. The first version becomes very expensive computationally due to its integro-differential nature, and the second version requires careful treatment (to avoid spurious wave propagation), because two of its three governing equations are hyperbolic.

The third version of the vorticity–velocity formulation describes the velocity field using second order Poisson-like equations, which are derived by combining the curl of the definition of vorticity and the gradient of continuity. These Poisson-like equations, along with the vorticity transport equation, constitute an elliptic set of fluid-dynamic equations. In addition to avoiding the difficulty of pressure boundary condition specification, employing the third version of the formulation avoids the use of a staggered grid, on which variable interpolation and grid refinement can become complicated. The third version of the formulation is particularly attractive for calculations that use a fully implicit solver, such as Newton's method, since the second order elliptic nature of the equations allows an implicit solution to be achieved within a comparatively short CPU time. This approach (i.e., solving the third version of the vorticity–velocity formulation using a fully implicit solver) has been successfully applied to 3D steady compressible flows [5], flame calculations with detailed chemistry [6–8], flame calculations with soot modeling [9], chemical vapor deposition modeling [10], and unsteady laminar diffusion flames [11]. It should be noted that none of these applications had solid protrusions in the computational domain.

Dennis and Hudson [12] as well as Wen-Zhong and Ta-Phuoc [13] have both employed a hybrid of the second and third versions of the vorticity–velocity formulation, solving a Poisson-like equation for all but one of the velocity components and solving the continuity equation for the last velocity component to ensure that continuity is satisfied. Although continuity is explicitly satisfied, this method has drawbacks as well. Dennis and Hudson point out that this procedure is possible because boundary conditions are given for all velocity components for a closed domain. Wen-Zhong and Ta-Phuoc state that in many flow cases, selection of the velocity component for which the continuity equation is solved is nontrivial and can affect the numerical solution of the problem. Moreover, due to the first order form of the continuity equation, the favorable convergence properties of the (previously elliptic) set of equations may be lost. To overcome this last difficulty, a solution method using a fully implicit solver is presented by Ern and Smooke [5], in which the solution from the fully elliptic set of equations is used as the initial guess for the set of equations containing continuity. This

procedure is done to ensure mass conservation in the final solution and is successful when the generated initial guess is sufficiently close to the final solution.

Numerous other investigators have studied the difficulties in ensuring continuity when the vorticity–velocity formulation is used, and they have proposed various techniques to overcome the problem. Orlandi [14] uses an implicit time-splitting scheme and a staggered mesh to ensure mass conservation. Labidi and Ta-Phuoc [15] use an alternating direction implicit (ADI) algorithm to investigate flow over a circular cylinder using the Poisson-like velocity equations. They show that for low Reynolds flows only, when a fourth-order-accurate spatial discretization is used in the radial direction, continuity is better satisfied than with a second-order-accurate method. Other investigators including Daube [16] have employed the influence matrix technique on a staggered grid to ensure continuity. Daube also shows that satisfying the continuity equation is equivalent to satisfying the kinematic definition of the vorticity. In other words, if the numerical solution of the vorticity field can be strongly coupled to the curl of the numerical solution of the velocity field, then continuity will be satisfied. It is this property that forms the basis of Daube's influence matrix technique, which couples the boundary conditions for vorticity and velocity. This same property forms the basis for the modified vorticity–velocity formulation that is developed in the present work.

Because this modified formulation will be used in future work to simulate unsteady flames, an important constraint of the present work is to maintain an elliptic set of governing equations, since ellipticity is known to ensure favorable convergence properties for fully implicit solvers such as Newton's method. Although Orlandi [14] and others have been successful in satisfying continuity on a staggered grid, the present work employs a nonstaggered grid to avoid the added complexity of a second grid and the requisite variable interpolation. Another constraint of the present work is to use standard second order discretizations that result in a nine-point computational stencil. This constraint is applied to minimize storage requirements and CPU time associated with forming and solving the linear system within each iteration of Newton's method. Finally, a solution to the problem of ensuring mass conservation is sought that does not require excessive grid refinement, so that combustion applications with detailed chemistry (often 50 or more unknowns per grid point) can still be simulated with reasonable computational effort.

In the remainder of this paper, a modified vorticity–velocity formulation is presented that effectively eliminates the lack of continuity previously observed in flow domains with solid protrusions. The modified vorticity–velocity formulation of the fluid-dynamic equations, when used with a fully implicit solver, can now be applied to problems in a broader range of geometrical configurations with extreme ease of implementation. In Section 2, the modified formulation is presented with the relevant boundary conditions. Discretization techniques and numerical solution methods are described in Section 3. In Section 4, it is shown that the existing vorticity–velocity formulation is insufficient for modeling the case of incompressible, axisymmetric flow through a suddenly expanding pipe. The modified formulation is then applied, and the computed reattachment length is shown to compare favorably to experimental results. The modified formulation is subsequently applied to a confined, axisymmetric laminar partially premixed methane–air flame with detailed chemistry and multicomponent transport, generated on a burner whose inner tube extends above the burner surface. The computed solution shows a significant improvement when compared with results from the application of the unmodified formulation to the same flame. Finally, Section 5 presents conclusions and some suggestions for future research.

2. Problem formulation

2.1. Governing equations

We begin with the conservation equations of mass and momentum for steady laminar flow [17]. Here, ρ is the density, v is the velocity vector, g is the gravitational acceleration, p is the pressure, and τ is the viscous stress tensor. The thermodynamic pressure is assumed constant since flows with low Mach number will be considered.

Continuity:

$$\nabla \cdot (\rho v) = 0. \tag{1}$$

Conservation of momentum:

$$\rho(v\cdot\nabla)v = -\nabla p + \nabla\cdot\tau + \rho g. \tag{2}$$

Neglecting the bulk viscosity coefficient, the viscous stress tensor can be written as

$$\tau_{ij} = \mu\left[\varepsilon_{ij} - \frac{2}{3}\delta_{ij}(\nabla\cdot v)\right], \tag{3}$$

where μ is the viscosity, $\varepsilon_{ij} = (\partial v_i/\partial x_j) + (\partial v_j/\partial x_i)$, and δ_{ij} is the identity tensor. The kinematic definition of vorticity is given by

$$\omega = \nabla\times v. \tag{4}$$

To form the vorticity transport equation, the curl of the momentum equation (2) is taken, eliminating the pressure gradient term. Any resulting terms having the form $\nabla\times v$ are replaced by ω, to produce the following elliptic equation.

Vorticity transport equation:

$$0 = -\mu\nabla^2\omega - \nabla\mu\times[2\nabla(\nabla\cdot v) - \nabla\times\omega] - \nabla\times[\varepsilon\cdot\nabla\mu] - \nabla\rho\times g + \nabla\rho\times[(v\cdot\nabla)v] + \rho[\nabla\times(\omega\times v)]. \tag{5}$$

To calculate the velocity field, either the Cauchy–Riemann system (Eqs. (1) and (4)) or Poisson-like velocity equations may be used. Poisson-like velocity equations are derived by substituting the curl of the vorticity definition (4) into the gradient of the product of $\frac{1}{\rho}$ and the continuity equation (1).

Poisson equation:

$$\nabla^2 v = -\nabla\times\omega - \nabla\left(\frac{v\cdot\nabla\rho}{\rho}\right). \tag{6}$$

The system of Eqs. (5) and (6) will be used as the foundation for the present work. A complete derivation of the vorticity transport and Poisson-like velocity equations may be found in [5].

In cylindrical coordinates, the commonly used version of the vorticity–velocity formulation with Poisson-like velocity equations is obtained when (5) and (6) are rewritten as follows, where v_r and v_z represent the radial and axial velocity components, respectively.

Radial velocity equation:

$$\frac{\partial^2 v_r}{\partial r^2} + \frac{\partial^2 v_r}{\partial z^2} = \frac{\partial\omega}{\partial z} - \frac{\partial}{\partial r}\left(\frac{v_r}{r}\right) - \frac{\partial}{\partial r}\left(\frac{v\cdot\nabla\rho}{\rho}\right). \tag{7}$$

Axial velocity equation:

$$\frac{\partial^2 v_z}{\partial r^2} + \frac{\partial^2 v_z}{\partial z^2} = -\frac{\partial\omega}{\partial r} - \frac{1}{r}\frac{\partial v_r}{\partial z} - \frac{\partial}{\partial z}\left(\frac{v\cdot\nabla\rho}{\rho}\right). \tag{8}$$

Vorticity transport equation:

$$\begin{aligned}\frac{\partial^2(\mu\omega)}{\partial r^2} + \frac{\partial^2(\mu\omega)}{\partial z^2} = {} & -\frac{\partial}{\partial r}\left(\frac{\mu\omega}{r}\right) + \rho v_r\frac{\partial\omega}{\partial r} + \rho v_z\frac{\partial\omega}{\partial z} - \frac{\rho v_r\omega}{r} + \overline{\nabla}\rho\cdot\nabla\left(\frac{v\cdot v}{2}\right) - \overline{\nabla}\rho\cdot g \\ & + 2\left(\overline{\nabla}(\mathrm{div}(v))\cdot\nabla\mu - \nabla v_r\cdot\overline{\nabla}\frac{\partial\mu}{\partial r} - \nabla v_z\cdot\overline{\nabla}\frac{\partial\mu}{\partial z}\right).\end{aligned} \tag{9}$$

Eq. (9) makes use of the notation below

$$\mathrm{div}(v) = \frac{1}{r}\frac{\partial(rv_r)}{\partial r} + \frac{\partial v_z}{\partial z}, \quad \overline{\nabla}\beta = \frac{\partial\beta}{\partial z} - \frac{\partial\beta}{\partial r}.$$

Eqs. (7)–(9) will be referred to as the "unmodified vorticity–velocity formulation". The kinematic definition of vorticity (4), when written in cylindrical coordinates, is

$$\omega = \frac{\partial v_r}{\partial z} - \frac{\partial v_z}{\partial r}. \tag{10}$$

Modified versions of the two equations are derived when definition (10) is inserted into the radial and axial velocity equations, (7) and (8), within the $\frac{\partial \omega}{\partial z}$ and $\frac{\partial \omega}{\partial r}$ terms, respectively.

Modified radial velocity equation:

$$\frac{\partial^2 v_r}{\partial r^2} = -\frac{\partial^2 v_z}{\partial z \partial r} - \frac{\partial}{\partial r}\left(\frac{v_r}{r}\right) - \frac{\partial}{\partial r}\left(\frac{v \cdot \nabla \rho}{\rho}\right). \tag{11}$$

Modified axial velocity equation:

$$\frac{\partial^2 v_z}{\partial z^2} = -\frac{\partial^2 v_r}{\partial r \partial z} - \frac{1}{r}\frac{\partial v_r}{\partial z} - \frac{\partial}{\partial z}\left(\frac{v \cdot \nabla \rho}{\rho}\right). \tag{12}$$

It should be noted that Eqs. (11) and (12) could also have been derived by taking the radial and axial derivatives, respectively, of the product of $\frac{1}{\rho}$ and Eq. (1). Definition (10) is also substituted into (9) in the $\frac{\partial}{\partial r}(\frac{\mu\omega}{r})$ and $\frac{\rho v_r \omega}{r}$ terms to yield the modified version of (9) given below.

Modified vorticity transport equation:

$$\begin{aligned}\frac{\partial^2(\mu\omega)}{\partial r^2} + \frac{\partial^2(\mu\omega)}{\partial z^2} = &-\frac{\partial}{\partial r}\left(\frac{\mu}{r}\frac{\partial v_r}{\partial z}\right) + \frac{\partial}{\partial r}\left(\frac{\mu}{r}\frac{\partial v_z}{\partial r}\right) + \rho v_r \frac{\partial \omega}{\partial r} + \rho v_z \frac{\partial \omega}{\partial z} - \frac{\rho v_r}{r}\left(\frac{\partial v_r}{\partial z} - \frac{\partial v_z}{\partial r}\right) \\ &+ \overline{\nabla}\rho \cdot \nabla\left(\frac{v \cdot v}{2}\right) - \overline{\nabla}\rho \cdot g + 2(\overline{\nabla}(\mathrm{div}(v)) \cdot \nabla\mu - \nabla v_r \cdot \overline{\nabla}\frac{\partial \mu}{\partial r} - \nabla v_z \cdot \overline{\nabla}\frac{\partial \mu}{\partial z}).\end{aligned} \tag{13}$$

The "modified vorticity–velocity formulation" consists of either the set of Eqs. (7), (12) and (13), or the set (11), (8) and (13). Both (11) and (12) should not be used as part of the same formulation since they can both be derived from Eq. (1). If *both* (11) and (12) were to be used, two variables (v_r and v_z) would be solved from a set of two equations, which were derived from only one original equation, and favorable convergence properties would be lost. (Recall that Eqs. (7) and (8) could be used in the same formulation because their derivation makes use of both Eqs. (1) and (4).) For the remainder of the present work, Eqs. (7), (12) and (13) are used as the "modified vorticity–velocity formulation", and the reason for their success is described in more detail in the second half of Section 4.1.

For nonreacting flows, appropriate boundary conditions are needed to complete the problem definition. In the first application examined in this paper (see Sections 2.2 and 4.1), assumptions have been made of constant density, constant viscosity, and negligible gravitational effects, leading to appropriate simplification of the fluid-dynamic equations.

For reacting flows, however, such as that studied in the second application of this paper (see Sections 2.3 and 4.2), not only are appropriate boundary conditions required, but the unsimplified fluid-dynamic equations are supplemented by the energy and species conservation equations, given below. Here, T is the temperature, λ is the thermal conductivity of the reacting gas mixture, N_{spec} is the total number of chemical species in the mixture, Y_n is the mass fraction of the nth species, $V_{n,r}$ and $V_{n,z}$ are the diffusion velocities of the nth species in the r and z directions, respectively, h_n is the specific enthalpy of the nth species, $c_{\mathrm{p},n}$ is the constant-pressure specific heat capacity of the nth species, c_{p} is the specific constant-pressure heat capacity of the mixture, W_n is the molecular weight of the nth species, $\dot{w}_n$ is the molar production rate of the nth species per unit volume, and $\nabla \cdot q_{\mathrm{R}}$ is the divergence of the net radiative flux per unit volume of the mixture.

Energy equation:

$$\begin{aligned}\rho c_{\mathrm{p}}\left(v_r \frac{\partial T}{\partial r} + v_z \frac{\partial T}{\partial z}\right) = &\frac{1}{r}\frac{\partial}{\partial r}\left(r\lambda \frac{\partial T}{\partial r}\right) + \frac{\partial}{\partial z}\left(\lambda \frac{\partial T}{\partial z}\right) - \sum_{n=1}^{N_{\mathrm{spec}}}\left[\rho c_{\mathrm{p},n} Y_n\left(V_{n,r}\frac{\partial T}{\partial r} + V_{n,z}\frac{\partial T}{\partial z}\right)\right] - \sum_{n=1}^{N_{\mathrm{spec}}} h_n W_n \dot{w}_n \\ &+ \nabla \cdot q_{\mathrm{R}} + \mu\left[2\left(\frac{\partial v_r}{\partial r}\right)^2 + 2\left(\frac{v_r}{r}\right)^2 + 2\left(\frac{\partial v_z}{\partial z}\right)^2 + \left(\frac{\partial v_r}{\partial z} + \frac{\partial v_z}{\partial r}\right)^2 - \frac{2}{3}(\mathrm{div}(v))^2\right].\end{aligned} \tag{14}$$

Species equation for all reacting species (for $n = 1, 2, \ldots, N_{\text{spec}} - 1$*):*

$$\rho v_r \frac{\partial Y_n}{\partial r} + \rho v_z \frac{\partial Y_n}{\partial z} = -\frac{1}{r}\frac{\partial}{\partial r}(r\rho Y_n V_{n,r}) - \frac{\partial}{\partial z}(\rho Y_n V_{n,z}) + W_n \dot{w}_n. \tag{15}$$

Excess species equation for inert N_{spec}*:*

$$Y_{N_{\text{spec}}} = 1 - \sum_{n=1}^{N_{\text{spec}}-1} Y_n. \tag{16}$$

Via the ideal gas law, the density can be expressed in terms of the temperature and the species mass fractions. The gas is assumed Newtonian and diffusion is Fickian: the nth species diffusion velocity, $V_n = (V_{n,r}, V_{n,z})$, is given by $V_n = -D_n \nabla \ln Y_n$, where D_n is the diffusion coefficient of the nth species. The Soret and Dufour effects are neglected; viscous dissipation, however, is not neglected. The flow's small Mach number implies that the pressure field can be obtained via the ideal gas law. The chemical mechanism employed is GRI-Mech version 2.11 with all nitrogen-containing species removed, except for N_2 (the excess species in Eq. (16)), resulting in 31 species and 173 reversible reactions [18]. All thermodynamic, chemical, and transport properties are evaluated using CHEMKIN [19,20] and TPLIB [21,22] subroutine libraries, parts of which have been rewritten and restructured for greater speed [23]. The divergence of the net radiative flux, $\nabla \cdot q_R$, is calculated using an optically thin radiation submodel with three radiating species (H_2O, CO, and CO_2), the details of which are found in [24–26]. For a more detailed explanation of the reacting flow model, see [27].

2.2. Boundary conditions: incompressible, nonreacting flow

The first application to be studied is that of steady, incompressible, axisymmetric, laminar flow in a suddenly expanding pipe. Fig. 1(a) shows the pipe, into which the flow enters at the bottom and exits at the top. Because the flow is axisymmetric, the computational domain is two-dimensional (i.e., the right half of Fig. 1(a)), bounded by the solid wall, the inflow plane, the outflow plane, and the axis of symmetry.

To complete the problem specification with either the unmodified formulation (Eqs. (7)–(9)), or the modified formulation (Eqs. (7), (12) and (13)), boundary conditions must be specified. On the surface of the solid wall, a no-slip boundary condition is imposed.

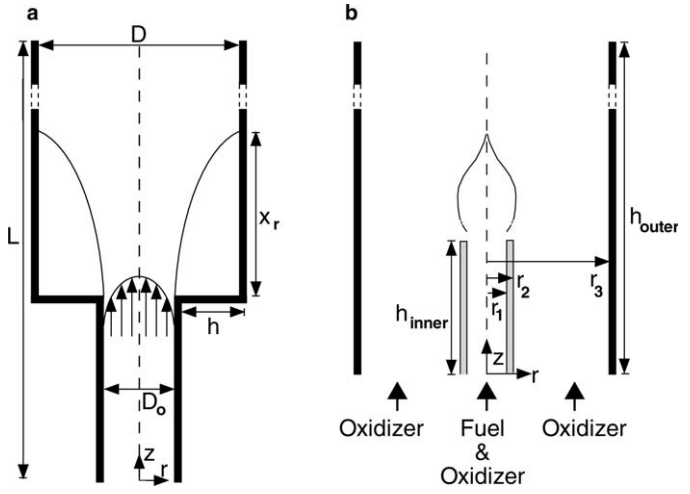

Fig. 1. (a) First application: laminar flow through an axisymmetric, suddenly expanding pipe, including coordinate orientation (not drawn to scale). The presence of the sudden change in pipe diameter generates high vorticity gradients. (b) Second application: axisymmetric laminar flame, including coordinate orientation (not drawn to scale). The presence of the extended inner tube to a height h_{inner} above the burner surface generates high vorticity gradients.

Wall surface:

$$v_r = 0, \quad v_z = 0, \quad \omega = \frac{\partial v_r}{\partial z} - \frac{\partial v_z}{\partial r}. \tag{17}$$

Note that for any wall to which r is the normal coordinate, $\frac{\partial v_r}{\partial z} = 0$, and for any wall to which z is the normal coordinate, $\frac{\partial v_z}{\partial r} = 0$, so the vorticity boundary condition in Eq. (17) can be simplified appropriately. The flow at the inlet is assumed to be parabolic and entirely axial.

Inflow:

$$v_r = 0, \quad v_z = v_{z_{\text{inlet}}}, \quad \omega = \frac{\partial v_r}{\partial z} - \frac{\partial v_z}{\partial r}. \tag{18}$$

Here,

$$v_{z_{\text{inlet}}} = 2v_{z_{\text{avg}}}\left[1 - \left(\frac{r}{D_o/2}\right)^2\right].$$

At the outlet, the flow is assumed to be fully developed, which is reflected in setting all the axial derivatives to zero.

Outflow:

$$\frac{\partial v_r}{\partial z} = 0, \quad \frac{\partial v_z}{\partial z} = 0, \quad \frac{\partial \omega}{\partial z} = 0. \tag{19}$$

This assumption is valid when the pipe is long enough, consistent with the analysis in [28]; indeed, all solutions presented here are independent of the length of the expanded diameter section of the pipe. Finally, the boundary conditions at the axis of symmetry are posed as follows.

Axis of symmetry:

$$v_r = 0, \quad \frac{\partial v_z}{\partial r} = 0, \quad \omega = 0. \tag{20}$$

It should be noted that the first derivatives in all boundary conditions are discretized carefully to achieve second-order discretization error, within the constraints of the nine-point computational stencil being used here. Details are presented in Section 3.1.

2.3. Boundary conditions: compressible, reacting flow

The second application to be studied is that of a confined, axisymmetric laminar flame at steady state with detailed chemistry and multicomponent transport, generated on a burner whose inner tube extends above the burner surface. In Fig. 1(b), fuel and oxidizer enter from below through the inner tube, air enters from below through the outer tube, and the flow exits at the top. This configuration generates a partially premixed flame, and the inlet flow rates and composition are such that the overall equivalence ratio (defined as the inner tube air flowrate required for complete combustion divided by the actual inner tube air flowrate) is 3.189. The computational domain includes the region between the burner surface and the top of the extended inner tube wall (as well as inside the tube wall itself) so that details of the fluid and temperature fields in this region are modeled. This inclusion is only necessary in cases where the flame sits so close to the top of the extended inner tube wall such that downward heat conduction is appreciable. Because the flow is again axisymmetric, the computational domain is two-dimensional (i.e., the right half of Fig. 1(b)), bounded by the solid outer wall, the inflow plane (comprising the two gas inlets and the bottom of the extended inner tube wall), the outflow plane, and the axis of symmetry. In Fig. 1(b), $r_1 = 0.38$ cm, $r_2 = 0.48$ cm, $r_3 = 4.7625$ cm, $h_{\text{inner}} = 2.54$ cm, and $h_{\text{outer}} = 40$ cm.

The governing equations consist of either the unmodified formulation, or the modified formulation, together with Eqs. (14)–(16), which are solved (for dependent variables v_r, v_z, ω, T, and Y_n, for $n = 1, \ldots, N_{\text{spec}}$) throughout the entire domain, except for the extended inner tube wall. Inside the extended inner tube wall

itself, which is made of steel, T is the only dependent variable. Thus, the only governing equation to be solved there is the heat conduction equation, with the following material properties for steel: $\lambda = 1620$ J/(cm K s); $c_p = 0.5018$ J/(g K); and $\rho = 8$ g/cm^3.

Boundary and interface conditions complete the problem specification. On the solid outer wall and the extended inner tube wall, no-slip boundary conditions and the corresponding vorticity boundary condition (17) are again imposed. The fluid boundary conditions are the same as those used in the incompressible, non-reacting flow case for the inflow, outflow, and the axis of symmetry, with the inlet velocity in (18) now specified as follows.

$$v_{z_{\text{inlet}}} = \begin{cases} 2v_{zi}\left[1 - \left(\frac{r}{r_1}\right)^2\right] & \text{for } 0 \leqslant r \leqslant r_1, \\ v_{zo}[1 - \exp(-\left|\frac{r-r_2}{\Delta}\right|) - \exp\left(-\left|\frac{r-r_3}{\Delta}\right|\right)] & \text{for } r_2 \leqslant r \leqslant r_3. \end{cases} \tag{21}$$

Here, $v_{zi} = 42$ cm/s, $v_{zo} = 20$ cm/s, and $\Delta = 0.02$ cm. Results are found to be insensitive to the choice of the parameter Δ, which controls the width of the fluid boundary layer in the outer inlet [29].

Temperature and species boundary conditions are specified as follows. A 3:1 molar ratio of air to methane (at room temperature) enters the domain through the inner tube, described by the following Dirichlet conditions.

Inflow through the inner tube:

$$T = 298 \text{ K}, \quad X_{\text{CH}_4} = 0.25, \quad X_{\text{O}_2} = 0.1568, \quad X_{\text{N}_2} = 0.5932, \quad \text{all other } X_n = 0. \tag{22}$$

Here, X_n is the molar fraction of the nth species. Mass fractions (appearing in Eq. (15)) are related to mole fractions by

$$Y_n = \frac{X_n W_n}{\sum_{j=1}^{N_{\text{spec}}} X_j W_j}.$$

Air at room temperature enters the domain through the outer tube, described by the following Dirichlet conditions.

Inflow through the outer tube:

$$T = 298 \text{ K}, \quad X_{\text{O}_2} = 0.209, \quad X_{\text{N}_2} = 0.791, \quad \text{all other } X_n = 0. \tag{23}$$

The base of the extended inner tube wall is held at a constant temperature of $T = 298$ K. At the opposite end of the domain, the outlet is assumed to be far enough from the reaction zone that all remaining axial derivatives of temperature and species mass fractions vanish.

Outflow:

$$\frac{\partial T}{\partial z} = 0, \quad \frac{\partial Y_n}{\partial z} = 0 \quad \text{for all } Y_n. \tag{24}$$

A no-flux condition is imposed at the surface of the solid outer wall.

Surface of the outer wall:

$$\frac{\partial T}{\partial r} = 0, \quad \frac{\partial Y_n}{\partial r} = 0 \quad \text{for all } Y_n. \tag{25}$$

The boundary conditions at the axis of symmetry are posed as follows.

Axis of symmetry:

$$\frac{\partial T}{\partial r} = 0, \quad \frac{\partial Y_n}{\partial r} = 0 \quad \text{for all } Y_n. \tag{26}$$

Since only the heat conduction equation is solved inside the extended inner tube wall, boundary conditions are required for species on its surface and an interface condition is required for temperature. It is assumed that the heat flux across the surface of the extended wall is continuous and that there is no species flux.

Surface of the extended inner tube wall:

$$\lambda_+ \left.\frac{\partial T}{\partial \hat{n}}\right|_+ = \lambda_- \left.\frac{\partial T}{\partial \hat{n}}\right|_-, \quad \left.\frac{\partial Y_n}{\partial \hat{n}}\right|_+ = 0. \tag{27}$$

Here, $\hat{n}$ is the outward pointing normal to the surface of the extended wall (i.e., $\hat{n} = -\hat{r}$ on the inside of the inner tube, $\hat{n} = \hat{r}$ on the outside of the inner tube, and $\hat{n} = \hat{z}$ at the top of the inner tube).

It should be noted that, for the reacting flow case, the first derivatives in all boundary conditions and in the interface condition are discretized such that second-order discretization error is achieved (as described in Section 3.1).

3. Numerical method

3.1. Discretization techniques

For each application considered here, the computational domain is discretized via a 2D tensor-product (structured) grid, having N_r points in the radial direction from the centerline to the part of the domain with the largest radius and N_z points in the axial direction from inflow to outflow. The total number of points, N_{points}, does not exceed $N_r \times N_z$.

The governing equations, as described in Section 2.1, are discretized at all interior grid points. First derivatives are discretized using centered differences that are second-order-accurate on uniform grids and between first- and second-order-accurate on nonuniform grids. Second derivatives are discretized using centered differences that are second-order-accurate on uniform grids and first-order-accurate on nonuniform grids. For convective terms, first-order upwind discretizations are employed. It should be noted that the discretizations only involve values at points that are nearest neighbors of the point at which the derivatives are being approximated. This strategy results in a computational stencil involving, at most, nine points. The Jacobian matrix within Newton's method (see Section 3.2) will therefore have a predetermined sparsity structure.

The boundary conditions, stated in Sections 2.2 and 2.3, are either Dirichlet or contain first derivatives. For the outflow boundary condition, the derivatives are approximated using second-order-accurate backward differences. However, for all other derivatives within all other boundary conditions, special treatment is required to produce a second-order-accurate discretization within the confines of the nine-point computational stencil. Second-order-accurate discretizations of the boundary conditions are necessary to obtain a mass-conserving solution (see Section 4.1). While a second-order-accurate discretization could be derived by using a wider computational stencil, such a discretization would adversely affect the predetermined sparsity structure of the Jacobian matrix.

The procedure for determining a second-order-accurate discretization is as follows. Consider, for example, the vorticity boundary condition along a solid outer wall to which r is the normal coordinate. The velocity and vorticity boundary conditions from Eq. (17) are given as

$$v_r = 0, \quad v_z = 0, \quad \omega = -\frac{\partial v_z}{\partial r}. \tag{28}$$

The derivation of a second-order-accurate discretization for $\frac{\partial v_z}{\partial r}$ at point (i,j), where i denotes the radial grid-point index and j denotes the axial grid-point index, begins by expanding v_z at point $(i-1,j)$ in a Taylor series about point (i,j)

$$v_z^{(i-1,j)} = v_z^{(i,j)} - \Delta r \frac{\partial v_z}{\partial r}^{(i,j)} + \frac{(\Delta r)^2}{2}\frac{\partial^2 v_z}{\partial r^2}^{(i,j)} - \frac{(\Delta r)^3}{6}\frac{\partial^3 v_z}{\partial r^3}^{(i,j)} + \cdots \tag{29}$$

Here, Δr is the local grid spacing in the radial direction, equal to $r_i - r_{i-1}$. The next step is to eliminate the second derivative from the Taylor expansion, by making use of the governing equation containing this particular second derivative. In the present work, discretizations of the boundary conditions remain unchanged between the unmodified and modified formulations. They are derived using the governing equations from the unmodified formulation only. For boundary condition (28), recall the unmodified axial velocity equation (8), which has been solved for the desired second derivative, below

$$\frac{\partial^2 v_z}{\partial r^2} = -\frac{\partial^2 v_z}{\partial z^2} - \frac{\partial \omega}{\partial r} - \frac{1}{r}\frac{\partial v_r}{\partial z} - \frac{\partial}{\partial z}\left(\frac{v \cdot \nabla \rho}{\rho}\right). \tag{30}$$

Eq. (30) is now applied at point (i,j). Since the wall is parallel to the z coordinate and the no-slip condition has been applied, $\frac{\partial^2 v_z}{\partial z^2} = 0$, $\frac{\partial v_r}{\partial z} = 0$ and $\frac{\partial}{\partial z}(\frac{v \cdot \nabla \rho}{\rho}) = 0$. Thus, at point (i,j), Eq. (30) reduces to

$$\frac{\partial^2 v_z}{\partial r^2}^{(i,j)} = -\frac{\partial \omega}{\partial r}^{(i,j)}. \tag{31}$$

Substituting (31) into (29) and rearranging for $\frac{\partial v_z}{\partial r}$ yields

$$\frac{\partial v_z}{\partial r}^{(i,j)} = \frac{v_z^{(i,j)} - v_z^{(i-1,j)}}{\Delta r} - \frac{\Delta r}{2}\frac{\partial \omega}{\partial r}^{(i,j)} - \frac{(\Delta r)^2}{6}\frac{\partial^3 v_z}{\partial r^3}^{(i,j)} + \cdots \tag{32}$$

Another Taylor series is now generated by expanding ω at point $(i-1,j)$ about point (i,j).

$$\omega^{(i-1,j)} = \omega^{(i,j)} - \Delta r\frac{\partial \omega}{\partial r}^{(i,j)} + \frac{(\Delta r)^2}{2}\frac{\partial^2 \omega}{\partial r^2}^{(i,j)} - \frac{(\Delta r)^3}{6}\frac{\partial^3 \omega}{\partial r^3}^{(i,j)} + \cdots \tag{33}$$

Eq. (33) is then solved for $\frac{\partial \omega}{\partial r}$, and the resulting expression is substituted into (32) to yield

$$\frac{\partial v_z}{\partial r}^{(i,j)} = \frac{v_z^{(i,j)} - v_z^{(i-1,j)}}{\Delta r} - \frac{\Delta r}{2}\left[\frac{\omega^{(i,j)} - \omega^{(i-1,j)}}{\Delta r} + \frac{\Delta r}{2}\frac{\partial^2 \omega}{\partial r^2}^{(i,j)} + \cdots\right] - \frac{(\Delta r)^2}{6}\frac{\partial^3 v_z}{\partial r^3}^{(i,j)} + \cdots$$

Terms with powers in Δr of two or greater are then truncated, and $v_z^{(i,j)}$ is set to zero due to the no-slip condition, thus generating the desired second-order-accurate discretization:

$$\frac{\partial v_z}{\partial r}^{(i,j)} \approx -\frac{v_z^{(i-1,j)}}{\Delta r} - \frac{\omega^{(i,j)} - \omega^{(i-1,j)}}{2}. \tag{34}$$

A similar procedure is applied to all other boundary conditions that contain first derivatives (with the exception of the outflow condition since second-order-accuracy is achieved there without this procedure). In order to derive the second-order-accurate discretizations of the temperature and species boundary conditions that appear in the reacting flow application, Eqs. (14) and (15) are used, respectively, to obtain relationships analogous to (31), which are then combined with the appropriate Taylor series expansions. In order to discretize the two first derivatives of temperature that appear in the interface condition (27), the same strategy is employed, making use of the energy equation in the gaseous region of the domain and the steady-state heat conduction equation in the solid steel region of the domain.

3.2. Solution method

Once the coupled, nonlinear system of equations has been discretized as described in the previous section, a discrete solution must be obtained on the 2D, tensor-product grid for all of the dependent variables. The problem contains a total of N_{dep} dependent variables at each grid point, where $N_{\text{dep}} = 3$ for the nonreacting flow case (v_r, v_z and ω) and $N_{\text{dep}} = 4 + N_{\text{spec}}$ for the reacting flow case (v_r, v_z, ω, T, and Y_n, for $n = 1, \ldots, N_{\text{spec}}$). The discretized equations are cast in residual form as follows:

$$F(U) = 0, \tag{35}$$

where U is an $N_{\text{points}} \times N_{\text{dep}}$ matrix of all the unknowns at all the grid points. This nonlinear system is then iteratively solved using a damped modified Newton's method, in which the kth iteration takes the form

$$J(U^k)(U^{k+1} - U^k) = -\lambda^k F(U^k). \tag{36}$$

Here, λ^k is the kth damping parameter [30], and $J(U^k)$ is the Jacobian matrix, whose predetermined sparsity structure (based on the nine-point computational stencil being used) has no more than nine nonzero block entries in any block row or block column.

If the solution is converging quickly enough at a given Newton iteration, as determined by theoretical estimates [31], then the Jacobian can be reused in the next iteration, thus reducing the number of Jacobian evaluations. Within each Newton iteration, the linear system is solved using a Bi-CGSTAB linear solver [32] with a block Gauss–Seidel preconditioner.

In general, the numerical procedure begins by adding a pseudo-transient term to one or more of the governing equations, thus temporarily casting the original nonlinear elliptic equations into parabolic form. Backward differences are used to discretize the pseudo-time terms, and Newton's method (as described above) solves the system at each pseudo-time level. When a specified number of adaptively chosen pseudo-time steps [33] has been completed, all pseudo-transient terms are removed, and Newton iterations continue until a steady-state solution is generated. Convergence is achieved when the 2-norm of a scaled correction vector is reduced beyond a prescribed tolerance. The combined pseudo-transient and steady-state solution procedure is discussed in greater detail in [34].

4. Results and discussion

4.1. Computational results – incompressible nonreacting flow

All calculations for the case of nonreacting flow were performed on a 2.0 GHz Opteron processor with 5 GB RAM. The prescribed convergence tolerance for Newton's method (see Section 3.2) was set to 10^{-6}. Since continuity is not explicitly satisfied in either the unmodified formulation or the modified formulation, the degree of accuracy to which a converged solution will obey continuity is not known a priori. As a measure of how closely continuity is satisfied, the mass loss for each converged solution will be computed according to

$$ML = \max_{j=1,2,\ldots,N_z}\left(1-\frac{\Phi_j}{\Phi_1}\right). \tag{37}$$

Here, Φ_j is the axial mass flux at pipe cross-section j, calculated from $\Phi_j = \left[\int_A (\rho v_z)\,\mathrm{d}A\right]_j$ using the trapezoidal rule, where A is the cross-sectional area of the domain through which the mass flux is calculated. (Negative values denote a mass gain.)

When the unmodified formulation is discretized and solved on a uniform base grid of $N_r = 21$ and $N_z = 181$, the converged solution displays a mass loss of 97.17% (i.e., $(\Phi_j/\Phi_1)_{\min} = 0.0283$). In order to test the effect of grid spacing, solutions are also computed on five finer grids (up to $N_r = 91$ and $N_z = 811$) that maintain the same cell aspect ratio as the base grid. The results are shown in Fig. 2(a) for an upstream Reynolds number of 83.2, where $Re = \rho v_{z_{\mathrm{avg}}} D_{\mathrm{o}}/\mu$. The plot yields the following relationship between mass loss

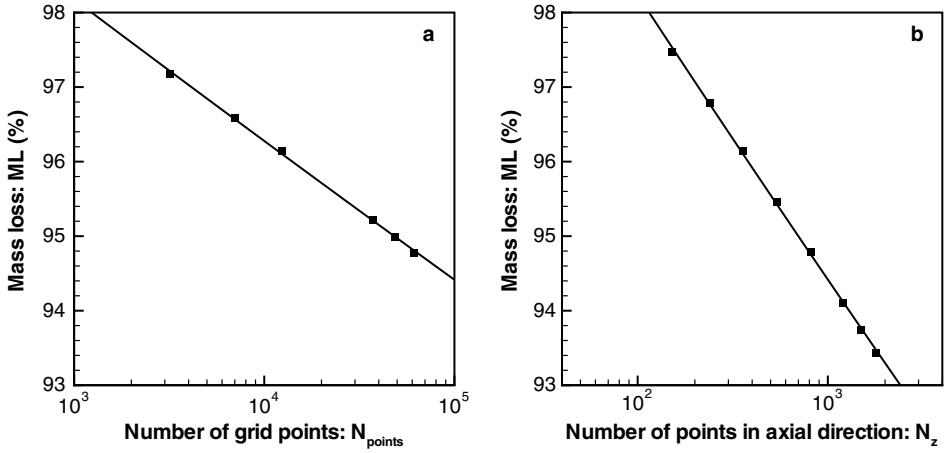

Fig. 2. (a) Axisymmetric pipe flow with sudden expansion: mass loss as a function of total number of grid points at constant cell aspect ratio when the unmodified vorticity–velocity formulation is employed. Equation of the least-squares-fitted line: $ML = 103.8 - 0.81 \times \ln(N_{\mathrm{points}})$. $Re = 83.2$. (b) Mass loss as a function of N_z at constant N_r when the unmodified vorticity–velocity formulation is employed. Equation of the least-squares-fitted line: $ML = 105.8 - 1.6 \times \ln(N_z)$. $Re = 83.2$.

and N_{points}: $ML = 103.8 - 0.81 \times \ln(N_{\text{points}})$. When the data are extrapolated to zero mass loss, full adherence to continuity would require a grid that is far beyond the limits set by storage and computational capabilities. Further investigation shows that this result is independent of cell aspect ratio.

Mass loss obtained using the unmodified formulation is plotted as a function of the number of points in the axial direction in Fig. 2(b). The plot yields the following relationship between mass loss and N_z: $ML = 105.8 - 1.6 \times \ln(N_z)$. For this and various other values of N_r, mass loss is a function of $(\Delta z)^{1.6}$, since $\Delta z \propto N_z^{-1}$. This dependence is not unexpected due to the fact that the discretization scheme contains first- to second-order-accurate discretizations, as described in Section 3.1. When Δz is held constant and Δr is varied, mass loss exhibits a weaker dependence on radial spacing, from which it can be concluded that the local discretization error is dominated by axial terms. Further tests show that the presence of substantial mass loss is unaffected by increasing the length of the computational domain.

When the modified formulation is employed, however, continuity *is* satisfied. A striking example of this improvement is shown in Fig. 3(a), where the unmodified formulation exhibits almost no flow after the pipe diameter expansion, as compared with the modified formulation. With the modified formulation, larger velocities are visible near the pipe centerline, as expected, and a recirculation zone appears just downstream of the sudden expansion. Fig. 3(b) compares radial velocity profiles at $z = 6.2$ cm between the unmodified and modified formulations. It can be seen that although the overall shapes of the radial velocity profiles are similar, the average magnitude of the radial velocity is much smaller with the unmodified formulation than with the modified formulation. Fig. 3(c) compares axial velocity profiles at $z = 6.2$ cm between the unmodified and modified formulations. The modified formulation exhibits a well-developed velocity profile with noticeable

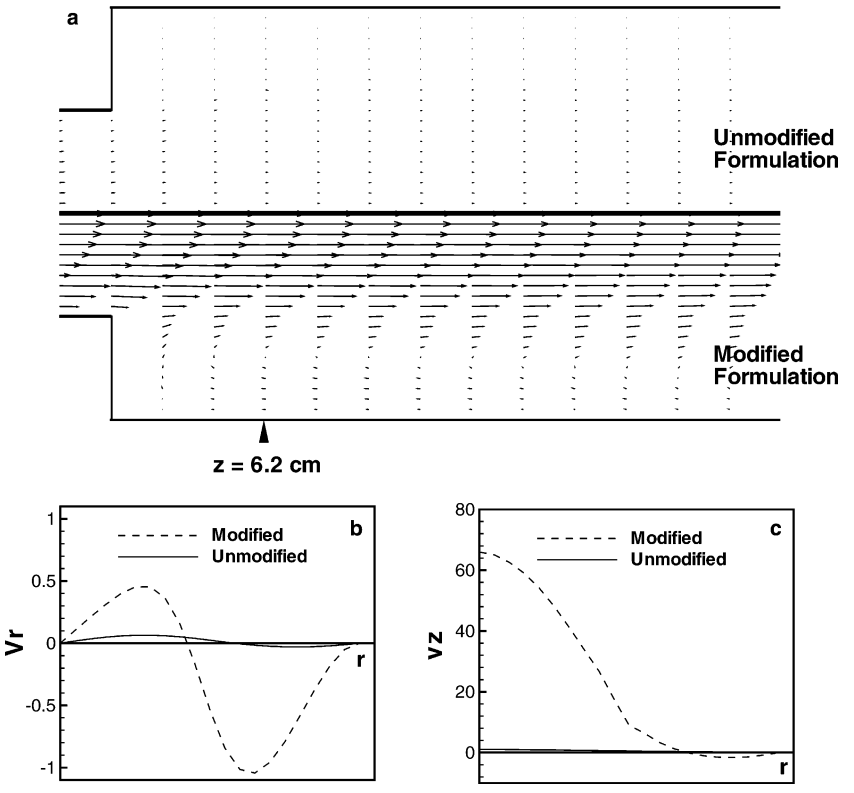

Fig. 3. Axisymmetric pipe flow with sudden expansion: (a) Comparison of recirculation after the pipe expansion between the unmodified formulation (upper) and modified formulation (lower). One fortieth of the axial pipe length is shown here. For greater clarity, velocity vectors are shown at only one sixteenth of the grid points. The same vector length scale is used in both halves of the figure. $N_r = 81$, $N_z = 721$, $Re = 83.2$. (b) Comparison of radial velocity profiles between the unmodified and modified formulations after the pipe expansion at $z = 6.2$ cm. (c) Comparison of axial velocity profiles between the unmodified and modified formulations after the pipe expansion at $z = 6.2$ cm.

recirculation, whereas axial velocity in the unmodified formulation is monotonically decreasing from the centerline outward and exhibiting much smaller velocity magnitudes. Fig. 4 compares normalized axial mass flux for the unmodified and modified formulations on a grid with $N_r = 41$ and $N_z = 361$, from which it can be seen that mass is conserved (mass loss of 0.52%) when the modified formulation is employed. This figure also shows that axial mass flux decreases at a constant rate with respect to z, up to the pipe expansion, in the unmodified formulation. This behavior implies that the amount by which continuity is dissatisfied is independent of z, since the graph shows the same rate of mass loss at each axial position.

This linear decrease in mass flux can be understood when the governing equations of the unmodified formulation are examined more carefully. The derivation process of the unmodified formulation is represented schematically by Eq. (38), where (38a) represents (7) and (38b) represents (8). The solution of Eq. (7) in the unmodified formulation implies that either both equalities in (38a) are satisfied, or that neither is satisfied. In addition, the solution of Eq. (8) implies that either both equalities in (38b) are satisfied, or that neither is satisfied. It is important to recall that Eqs. (7) and (8) are also used in the process of deriving second-order-accurate discretizations of the boundary conditions (for both formulations).

$$\frac{\partial \omega}{\partial z} = \frac{\partial}{\partial z}(\nabla \times v) \text{ substituted into } \frac{\partial}{\partial r}\left(\frac{1}{\rho}\nabla \cdot (\rho v)\right) = 0, \tag{38a}$$

$$\frac{\partial \omega}{\partial r} = \frac{\partial}{\partial r}(\nabla \times v) \text{ substituted into } \frac{\partial}{\partial z}\left(\frac{1}{\rho}\nabla \cdot (\rho v)\right) = 0. \tag{38b}$$

Since $\frac{\partial}{\partial r}(\frac{1}{\rho}\nabla \cdot (\rho v)) = 0$ implies that $\frac{1}{\rho}\nabla \cdot (\rho v) = f(z)$ and since $\frac{\partial}{\partial z}(\frac{1}{\rho}\nabla \cdot (\rho v)) = 0$ implies that $\frac{1}{\rho}\nabla \cdot (\rho v) = f(r)$, it is reasonable to assume that the observed result in Fig. 4 (i.e., that mass loss for the unmodified formulation is dependent on r only) is caused by $\frac{\partial}{\partial r}(\frac{1}{\rho}\nabla \cdot (\rho v)) = 0$ being unsatisfied. However, the fact that (38a) *as a whole* is satisfied by the converged solution implies either that both of $\frac{\partial \omega}{\partial z} = \frac{\partial}{\partial z}(\nabla \times v)$ and $\frac{\partial}{\partial r}(\frac{1}{\rho}\nabla \cdot (\rho v)) = 0$ are satisfied or that neither is satisfied. The axial derivative of vorticity, $\frac{\partial \omega}{\partial z} = \frac{\partial}{\partial z}(\nabla \times v)$, must therefore also remain unsatisfied.

The derivation process of the modified formulation is represented schematically by Eq. (39), where (39a) represents the unmodified radial velocity equation (7), and Eq. (39b) represents the modified axial velocity equation (12). The solution of Eq. (7) in the modified formulation implies that either both equalities in (39a) are satisfied, or that neither is satisfied. The solution of Eq. (12) only requires satisfying the single equality in (39b). Eqs. (39c) and (39d) represent Eqs. (7) and (8), respectively, which are used in the process of deriving the discretizations of the boundary conditions (for both formulations). The incorporation of these discretizations into the modified formulation thus necessitates that either both equalities in (39d) are satisfied, or that neither is satisfied. The equivalent requirement for (39c) already exists due to the use of Eq. (7) in the modified formulation, represented schematically by Eq. (39a):

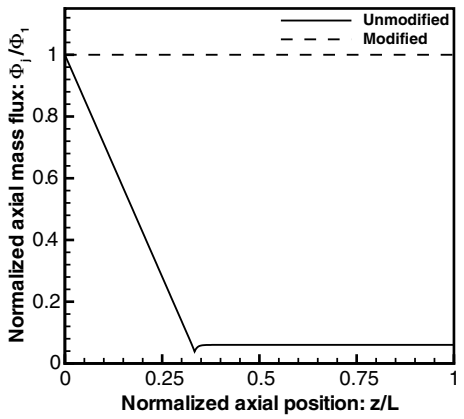

Fig. 4. Axisymmetric pipe flow with sudden expansion: comparison of axial mass flux as a function of axial position between the unmodified vorticity–velocity formulation and the modified vorticity–velocity formulation. At $z/L = 1$, $\Phi_j/\Phi_1 = 0.056$ for the unmodified formulation, and $\Phi_j/\Phi_1 = 1.001$ for the modified formulation. $Re = 83.2$.

$$\frac{\partial\omega}{\partial z} = \frac{\partial}{\partial z}(\nabla \times v) \text{ substituted into } \frac{\partial}{\partial r}\left(\frac{1}{\rho}\nabla\cdot(\rho v)\right) = 0, \tag{39a}$$

$$\frac{\partial}{\partial z}\left(\frac{1}{\rho}\nabla\cdot(\rho v)\right) = 0 \text{ only}, \tag{39b}$$

$$\frac{\partial\omega}{\partial z} = \frac{\partial}{\partial z}(\nabla \times v) \text{ substituted into } \frac{\partial}{\partial r}\left(\frac{1}{\rho}\nabla\cdot(\rho v)\right) = 0, \tag{39c}$$

$$\frac{\partial\omega}{\partial r} = \frac{\partial}{\partial r}(\nabla \times v) \text{ substituted into } \frac{\partial}{\partial z}\left(\frac{1}{\rho}\nabla\cdot(\rho v)\right) = 0. \tag{39d}$$

Since a converged solution for the modified formulation requires that $\frac{\partial}{\partial z}(\frac{1}{\rho}\nabla\cdot(\rho v)) = 0$ from (39b), $\frac{\partial\omega}{\partial r} = \frac{\partial}{\partial r}(\nabla\times v)$ must also be satisfied from (39d). The equality $\omega = \nabla\times v$ must also be satisfied from radial integration of both sides of $\frac{\partial\omega}{\partial r} = \frac{\partial}{\partial r}(\nabla\times v)$, which yields $\omega + g(z) = \nabla\times v$, where $g(z) = 0$ at every axial position since the kinematic definition of vorticity is identically satisfied by the boundary conditions imposed along the axis of symmetry. From (39a) and (39c) it must follow that $\frac{\partial}{\partial r}(\frac{1}{\rho}\nabla\cdot(\rho v)) = 0$. Since it is now the case that both $\frac{\partial}{\partial r}(\frac{1}{\rho}\nabla\cdot(\rho v)) = 0$ and $\frac{\partial}{\partial z}(\frac{1}{\rho}\nabla\cdot(\rho v)) = 0$, it follows that $\frac{1}{\rho}\nabla\cdot(\rho v) = C$, where C is a constant everywhere in the domain. Because of the particular boundary conditions imposed, continuity is identically satisfied at both $(i,j) = (N_r, 1)$, the point at the largest radial position along the inflow plane, and $(1, N_z)$, the point along the centerline at the outflow. Therefore, $C = 0$, and continuity is satisfied. Note that only in the modified formulation do cross derivatives of velocity necessarily appear. Without these cross derivatives in the formulation, the fluid-dynamic variables at $(N_r, 1)$ and $(1, N_z)$ would not appear within the computational stencil at any other point in the domain, and the null values of C at these two corner points would be decoupled from the setting of C (possibly to a nonzero value) in the rest of the domain. Thus, the presence of velocity cross derivatives, and their broadening effect on the computational stencil, is essential to the success of the modified formulation.

The simulation with the modified vorticity–velocity formulation is repeated for numerous Reynolds numbers. Nondimensionalized reattachment length x_r/h (as shown in Fig. 1(a)) is calculated as the axial position where $\omega = 0$ along the portion of the wall after the step [35], and it is plotted versus Reynolds number in Fig. 5. For the range of Reynolds values studied here, excellent agreement is seen between the experimental results of Macagno and Hung[35] and the results computed using the modified formulation. Care is taken to ensure that the calculated values for reattachment length are independent of the number of grid points and the convergence tolerance.

4.2. Computational results – compressible, reacting flow

All calculations for the case of reacting flow were performed on a 2.0 GHz Opteron processor with 5 GB RAM. The prescribed convergence tolerance for Newton's method (see Section 3.2) was set at 10^{-4}. Calcula-

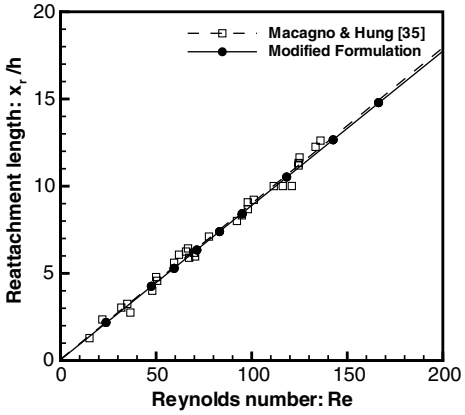

Fig. 5. Axisymmetric pipe flow with sudden expansion: comparison of reattachment length versus Reynolds number when the modified vorticity–velocity formulation is employed.

tions are performed on a nonuniform grid of $N_r = 145$ and $N_z = 311$, covering a domain of size 4.7625 cm × 40 cm. A small spacing is necessary to resolve the flame, but an equispaced grid could not be used due to memory limitations. Thus, in the radial direction, $\Delta r = 0.01$ cm from $r = 0$ cm to $r = 1.1$ cm. The spacing gradually increases to $\Delta r = 0.35$ cm at $r = 2.25$ cm and then gradually decreases, ending with $\Delta r = 0.01$ cm from $r = 4.7225$ cm to $r = 4.7625$ cm. In the axial direction, $\Delta z = 0.04$ cm at the bottom of the domain from $z = 0$ cm to $z = 0.2$ cm, which gradually increases to 0.06 cm at $z = 0.3$ cm. This Δz is maintained until $z = 1.06$ cm and then gradually decreases to $\Delta z = 0.015$ cm at $z = 2.42$ cm. At $z = 4.52$ cm, the spacing again begins a very gradual increase, and the largest Δz (2.0 cm) appears at the top of the domain, from $z = 30$ cm to $z = 40$ cm.

Here, a slightly different solution method than that used for the incompressible, nonreacting flow case is employed. First, the modified formulation (Eqs. (7), (12) and (13)) was used to obtain a solution, which contained 1.92% mass loss. This outcome was satisfactory, but it was found that an additional improvement could be made by substituting the modified radial velocity Eq. (11) for the unmodified Eq. (7), thereby employing all three modified equations. Convergence could only be obtained when the solution exhibiting 1.92% mass loss was used as the starting estimate for this additional run. The reasons for the difficulty in obtaining this convergence are discussed in Section 2.1. For the remainder of this section, results obtained using the additional run are presented and are referred to as having been generated by the 'modified formulation'.

Fig. 6 compares the computed normalized axial mass flux for simulations with the unmodified and modified formulations. It can be seen that use of the unmodified formulation produces a significant amount of mass loss, such that the mass exiting the top of the domain equals only one tenth of the mass entering the bottom of the domain. By contrast, the modified formulation generates almost no mass loss (mass gain of 0.12%), for the reasons outlined in the second half of Section 4.1. Fig. 6 shows a linear decrease in mass flux with respect to z, in a portion of the axial domain, which is also discussed in detail in Section 4.1.

Solution contours for three of the dependent variables are displayed in Fig. 7, where the unmodified formulation is shown on the left half of each picture and the modified formulation is shown on the right half of each picture. Fig. 7(a) shows the computed isotherms in a portion of the computational domain, with a maximum centerline temperature for the unmodified formulation of $T = 1952$ K, occurring at $z = 5.8$ cm, and a maximum centerline temperature for the modified formulation of $T = 1949$ K, occurring at $z = 6.7$ cm. Due to the unphysical reduction in axial mass flux obtained using the unmodified formulation, the location of the peak centerline temperature is considerably lower than that of the modified formulation. Although axial mass flux is reduced by 90% in the case employing the unmodified formulation, Fig. 6 indicates that much of this reduction occurs downstream of the region depicted in Fig. 7. As a consequence, the discrepancies in overall flame shape between the unmodified and modified formulations are diminished. For each formulation, Fig. 7(a) also shows the considerable amount of downward heat conduction into the solid inner tube

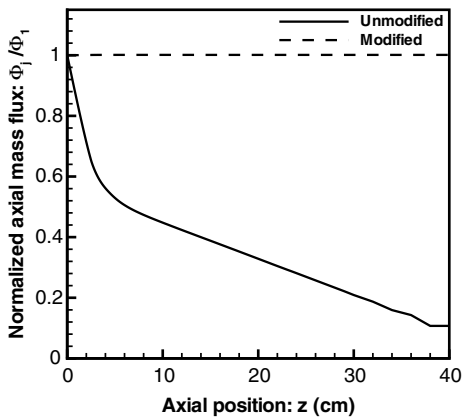

Fig. 6. Axisymmetric laminar flame: comparison of axial mass flux as a function of axial position between the unmodified vorticity–velocity formulation and the modified vorticity–velocity formulation. At $z/L = 1$, $\Phi_j/\Phi_1 = 0.107$ for the unmodified formulation, and $\Phi_j/\Phi_1 = 1.001$ for the modified formulation.

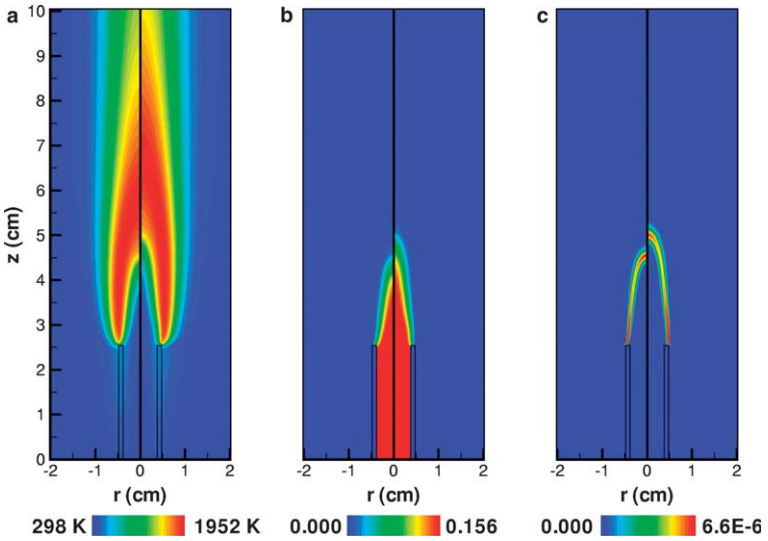

Fig. 7. Axisymmetric laminar flame: solution contours comparing the unmodified formulation (left half of each picture) with the modified formulation (right half of each picture). $N_r = 145$ and $N_z = 311$. Three of the 35 dependent variables are plotted in a portion of the computational domain. (a) Isotherms with a maximum centerline temperature for the unmodified formulation of $T = 1952$ K at $z = 5.8$ cm, and a maximum centerline temperature for the modified formulation of $T = 1949$ K at $z = 6.7$ cm. (b) Isopleths of mass fraction of methane (Y_{CH_4}). (c) Isopleths of mass fraction of the intermediate species C_2H_5 with a maximum centerline mass fraction for the unmodified formulation of $Y_{C_2H_5} = 6.6 \times 10^{-6}$ at $z = 4.56$ cm, and a maximum centerline mass fraction for the modified formulation of $Y_{C_2H_5} = 6.3 \times 10^{-6}$ at $z = 5.025$ cm. See text for additional details.

and surrounding fluid region. For example, the 400 K isotherm passes through the solid wall approximately 0.7 cm from its top edge. This heat conduction is one of two physical mechanisms responsible for the anchoring of the flame, the other being the presence of a wake immediately above the extended inner tube wall.

Fig. 7(b) shows isopleths of the methane mass fraction (Y_{CH_4}), with a maximum value for both the unmodified and modified formulations of $Y_{CH_4} = 0.156$ in the interior part of the inflow plane ($Y_{CH_4} = 0.156$ corresponds to $X_{CH_4} = 0.25$). Due to decreased axial mass flux in the unmodified formulation computations, methane consumption begins at a lower axial height than in the modified formulation, and the methane is almost completely consumed (i.e., $Y_{CH_4} \leqslant 1 \times 10^{-4}$) at $z = 5.4$ cm. In the modified formulation, however, Y_{CH_4} does not dip below 1×10^{-4} until $z = 6.2$ cm.

Fig. 7(c) shows mass fraction isopleths of C_2H_5, an intermediate compound whose behavior is typical of several minor species, which are formed inside the flame and quickly oxidized (burned). The maximum centerline mass fraction for the unmodified formulation is $Y_{C_2H_5} = 6.6 \times 10^{-6}$, occurring at $z = 4.56$ cm, and the maximum centerline mass fraction for the modified formulation is $Y_{C_2H_5} = 6.3 \times 10^{-6}$, occurring at $z = 5.025$ cm. Fig. 7(c) also clearly illustrates the lower flame position associated with the unmodified formulation – again attributable to the decreased mass flux. Because the modified formulation generates almost no mass loss, its solution is assumed to be more physically correct. However, further work involving experimental measurements would be required to determine the solution's physical accuracy.

5. Conclusions and future directions

In this paper, a modified vorticity–velocity formulation and some second-order-accurate boundary condition discretizations are derived and applied to two test cases: incompressible axisymmetric fluid flow through a suddenly expanding pipe; and a confined, axisymmetric laminar flame with detailed chemistry and multicomponent transport, generated on a burner whose inner tube extends above the burner surface. These two cases are chosen due to the presence of regions of high vorticity gradients, which previously have been observed to lead to unphysical solutions when the unmodified vorticity–velocity formulation is employed. For each test case, it is first shown that the unmodified vorticity–velocity formulation generates numerical solutions that

do not satisfy continuity. It is then shown that the modified formulation presented in this paper is capable of generating more physically accurate solutions that obey continuity to within a reasonable tolerance.

For the case of axisymmetric pipe flow presented here, the unphysical nature of the solution generated from the unmodified formulation is seen to be attributable neither to the grid parameters nor to the domain length. When the modified formulation is employed, however, continuity is satisfied and a visible recirculation zone is present. Moreover, the predicted reattachment lengths show excellent agreement with previously published experimental data for a variety of Reynolds numbers.

For the case of the axisymmetric laminar flame presented here, it is shown that when the modified vorticity–velocity formulation is combined with the conservation equations for temperature and chemical species, a solution that satisfies continuity can be generated – a result that is *not* observed when using the unmodified formulation. To the authors' knowledge, the computation employing the vorticity–velocity formulation presented here is the first published numerical solution to the axisymmetric laminar flame with detailed chemistry and multicomponent transport, generated on a burner whose inner tube extends above the burner surface.

Heading the list of future work related to the modified vorticity–velocity formulation is the task of comparing laminar flame solutions, similar to the one presented in this paper, to experimental data. Other future applications of the modified vorticity–velocity formulation include its implementation in different coordinate systems and in more complex geometrical configurations.

Acknowledgments

This work was supported in part by the US Department of Energy Office of Basic Energy Sciences (Grant No. DE-FG02-88ER13966) and the National Science Foundation (Grant No. CTS-0328296).

References

[1] Y. Xu, M.D. Smooke, Application of a primitive variable Newton's method for the calculation of an axisymmetric laminar diffusion flame, J. Comput. Phys. 104 (1993) 99–109.
[2] T.B. Gatski, Review of incompressible fluid flow computations using the vorticity–velocity formulation, Appl. Numer. Math. 7 (1991) 227–239.
[3] J.C. Wu, J.F. Thompson, Numerical solution of unsteady, three-dimensional Navier–Stokes equations, in: Proceedings, Project SQUID Workshop of Fluid Dynamics of Unsteady, Three-Dimensional and Separated Flows, Lafayette, IN, 1971, pp. 253–280.
[4] T.B. Gatski, C.E. Grosch, M.E. Rose, A numerical study of the two-dimensional Navier–Stokes equations in vorticity–velocity variables, J. Comput. Phys. 48 (1982) 1–22.
[5] A. Ern, M.D. Smooke, Vorticity–velocity formulation for three-dimensional steady compressible flows, J. Comput. Phys. 105 (1993) 58–71.
[6] A. Ern, Vorticity–velocity modeling of chemically reacting flows, Ph.D. Thesis, Yale University, New Haven, Mechanical Engineering Department, 1994.
[7] B.A.V. Bennett, M.D. Smooke, Local rectangular refinement with application to axisymmetric laminar flames, Combust. Theor. Model. 2 (1998) 221–258.
[8] B.A.V. Bennett, J. Fielding, R.J. Mauro, M.B. Long, M.D. Smooke, A comparison of the structures of lean and rich axisymmetric laminar Bunsen flames: application of local rectangular refinement solution-adaptive gridding, Combust. Theor. Model. 3 (1999) 657–687.
[9] M.D. Smooke, R.J. Hall, M.B. Colket, J. Fielding, M.B. Long, C.S. McEnally, L.D. Pfefferle, Investigation of the transition from lightly sooting towards heavily sooting co-flow ethylene diffusion flames, Combust. Theor. Model. 8 (2004) 593–606.
[10] A. Ern, C.C. Douglas, M.D. Smooke, Detailed chemistry modeling of laminar diffusion flames on parallel computers, Int. J. Supercomput. Appl. 9 (1995) 167–186.
[11] B.A.V. Bennett, M.D. Smooke, Unsteady axisymmetric laminar diffusion flames: an application of local rectangular refinement, in: Proceedings, 2001 Technical Meeting of the Eastern States Section of the Combustion Institute, The Combustion Institute, Hilton Head, SC, 2001, pp. 332–335.
[12] S.C.R. Dennis, J.D. Hudson, Methods of solution of the velocity–vorticity formulation of the Navier–Stokes equations, J. Comput. Phys. 122 (1995) 300–306.
[13] S. Wen-Zhong, L. Ta-Phuoc, Numerical method for unsteady 3D Navier–Stokes equations in velocity–vorticity form, Comput. Fluids 26 (1997) 193–216.
[14] P. Orlandi, Vorticity–velocity formulation for high Re flows, Comput. Fluids 15 (1987) 137–149.
[15] W. Labidi, L. Ta-Phuoc, Numerical resolution of the Navier–Stokes equations in velocity–vorticity formulation: application to the circular cylinder, in: Proceedings, 7th GAMM Conference on Numerical Methods in Fluid Dynamics, Vieweg, Braunschweig, 1988.

[16] O. Daube, Resolution of the 2D Navier–Stokes equations in velocity–vorticity form by means of an influence matrix technique, J. Comput. Phys. 103 (1992) 402–414.
[17] R.B. Bird, W.E. Stewart, E.N. Lightfoot, Transport Phenomena, Wiley, New York, 1960.
[18] C.T. Bowman, R.K. Hanson, D.F. Davidson, W.C. Gardiner Jr., V. Lissianski, G.P. Smith, M.D. Golden, M. Frenklach, H. Wang, M. Goldberg (1995). Available from: <http://www.gri.org>.
[19] R.J. Kee, J.A. Miller, T.H. Jefferson, Chemkin: a general-purpose, problem-independent, transportable, Fortran chemical kinetics code package, Sandia National Laboratory Report SAND80-8003, 1980.
[20] R.J. Kee, F.M. Rupley, J.A. Miller, The Chemkin thermodynamic database, Sandia National Laboratory Report SAND87-8215, 1987.
[21] R.J. Kee, J. Warnatz, J.A. Miller, A Fortran computer code package for the evaluation of gas-phase viscosities, conductivities, and diffusion coefficients, Sandia National Laboratory Report SAND83-8209, 1983.
[22] R.J. Kee, G. Dixon-Lewis, J. Warnatz, M.E. Coltrin, J.A. Miller, A Fortran computer package for the evaluation of gas-phase, multicomponent transport properties, Sandia National Laboratory Report SAND86-8246, 1986.
[23] V. Giovangigli, N. Darabiha, Vector computers and complex chemistry combustion, in: C.M. Brauner, C. Schmidt-Laine (Eds.), Mathematical Modeling in Combustion and Related Topics, Nijhoff, Dordrecht, 1988, pp. 491–503.
[24] D.K. Edwards, Molecular gas band radiation, Adv. Heat Transfer 12 (1976) 115–193.
[25] R.J. Hall, The radiative source term for plane-parallel layers of reacting combustion gases, J. Quantum Spectrosc. Radiat. Transfer 49 (1993) 517–523.
[26] R.J. Hall, The radiative dissipation in planar gas–soot mixtures, Quantum J. Spectrosc. Radiat. Transfer 51 (1994) 635–644.
[27] B.A.V. Bennett, C.S. McEnally, L.D. Pfefferle, M.D. Smooke, Computational and experimental study of axisymmetric coflow partially premixed methane/air flames, Combust. Flame 123 (2000) 522–546.
[28] H.L. Langhaar, Steady flow in the transition length of a straight tube, in: Transactions of the ASME, Lafayette, IN, 1942, vol. 64, pp. A55–A58.
[29] E. Burman, A. Ern, V. Giovangigli, Bunsen flame simulation by finite elements on adaptively refined, unstructured triangulations, Combust. Theor. Model. 8 (2004) 65–84.
[30] P. Deuflhard, Modified Newton's method for solution of ill-conditioned systems of nonlinear equations with application to multiple shooting, Numer. Math. 22 (1974) 289–315.
[31] M.D. Smooke, Error estimate for the modified Newton method with applications to the solution of nonlinear, two-point boundary-value problems, J. Optim. Theory Appl. 39 (1983) 489–511.
[32] H.A. Van Der Vorst, Bi-CGSTAB: a fast and smoothly converging variant of Bi-CG for the solution of nonsymmetric linear systems, SIAM J. Stat. Comput. 13 (1992) 631–644.
[33] M.D. Smooke, J.A. Miller, R.J. Kee, Solution of premixed and counterflow diffusion flame problems by adaptive boundary value methods, in: U.M. Ascher, R.D. Russell (Eds.), Numerical Boundary Value ODEs, Birkhäuser, Basel, 1985, pp. 303–317.
[34] M.D. Smooke, R.E. Mitchell, D.E. Keyes, Numerical solution of two-dimensional axisymmetric laminar diffusion flames, Combust. Sci. Tech. 67 (1989) 85–122.
[35] E.O. Macagno, T. Hung, Computational and experimental study of a captive annular eddy, J. Fluid Mech. 28 (1967) 43–64.